blood®
Regular Article

MYELOID NEOPLASIA

Aberrant *EVI1* splicing contributes to *EVI1*-rearranged leukemia

Atsushi Tanaka,[1,2] Taizo A. Nakano,[3] Masaki Nomura,[1,4] Hiromi Yamazaki,[1] Jan P. Bewersdorf,[5] Roger Mulet-Lazaro,[6,7] Simon Hogg,[5] Bo Liu,[5] Alex Penson,[5] Akihiko Yokoyama,[8] Weijia Zang,[1,9] Marije Havermans,[6,7] Miho Koizumi,[10] Yasutaka Hayashi,[1] Hana Cho,[5] Akinori Kanai,[11,12] Stanley C. Lee,[13,14] Muran Xiao,[1,15] Yui Koike,[1] Yifan Zhang,[1,9] Miki Fukumoto,[1] Yumi Aoyama,[1,9] Tsuyoshi Konuma,[16] Hiroyoshi Kunimoto,[17] Toshiya Inaba,[11] Hideaki Nakajima,[17] Hiroaki Honda,[10] Hiroshi Kawamoto,[2] Ruud Delwel,[6,7] Omar Abdel-Wahab,[5,*] and Daichi Inoue[1,*]

[1]Department of Hematology-Oncology, Institute of Biomedical Research and Innovation, Foundation for Biomedical Research and Innovation at Kobe, Kobe, Hyogo, Japan; [2]Laboratory of Immunology, Institute for Life and Medical Sciences, Kyoto University, Kyoto, Japan; [3]Department of Pediatrics, Section of Hematology, Oncology and Bone Marrow Transplantation, University of Colorado, Aurora, CO; [4]Facility for iPS Cell Therapy, CiRA Foundation, Kyoto, Japan; [5]Human Oncology and Pathogenesis Program, Memorial Sloan Kettering Cancer Center, New York, NY, United States; [6]Department of Hematology, Erasmus MC Cancer Institute, Rotterdam, The Netherlands; [7]Oncode Institute, Utrecht, The Netherlands; [8]Tsuruoka Metabolomics Laboratory, National Cancer Center, Yamagata, Japan; [9]Department of Hematology and Oncology, Graduate School of Medicine, Kyoto University, Kyoto, Japan; [10]Field of Human Disease Models, Major in Advanced Life Sciences and Medicine, Tokyo Women's Medical University, Tokyo, Japan; [11]Department of Molecular Oncology and Leukemia Program Project, Research Institute for Radiation Biology and Medicine, Hiroshima University, Hiroshima, Japan; [12]Department of Computational Biology and Medical Sciences, Graduate School of Frontier Sciences, The University of Tokyo, Chiba, Japan; [13]Clinical Research Division, Fred Hutchinson Cancer Center, Seattle, WA; [14]Department of Laboratory Medicine and Pathology, University of Washington, Seattle, WA; [15]Division of Cellular Therapy, The Institute of Medical Science, The University of Tokyo, Tokyo, Japan; [16]Structural Epigenetics Laboratory, and [17]Department of Stem Cell and Immune Regulation, Graduate School of Medicine, Yokohama City University, Yokohama, Kanagawa, Japan

KEY POINTS

- **A novel *EVI1* splice isoform is frequently expressed in inv(3)/t(3;3) leukemia and drives myeloid transformation.**
- **Frequent *SF3B1* mutations in inv(3)/t(3;3) leukemia generate a novel *EVI1* isoform with an altered second zinc finger domain.**

Detailed genomic and epigenomic analyses of *MECOM* (the MDS1 and EVI1 complex locus) have revealed that inversion or translocation of chromosome 3 drives inv(3)/t(3;3) myeloid leukemias via structural rearrangement of an enhancer that upregulates transcription of *EVI1*. Here, we identify a novel, previously unannotated oncogenic RNA-splicing derived isoform of *EVI1* that is frequently present in inv(3)/t(3;3) acute myeloid leukemia (AML) and directly contributes to leukemic transformation. This EVI1 isoform is generated by oncogenic mutations in the core RNA splicing factor SF3B1, which is mutated in >30% of inv(3)/t(3;3) myeloid neoplasm patients and thereby represents the single most commonly cooccurring genomic alteration in inv(3)/t(3;3) patients. *SF3B1* mutations are statistically uniquely enriched in inv(3)/t(3;3) myeloid neoplasm patients and patient-derived cell lines compared with other forms of AML and promote mis-splicing of EVI1 generating an in-frame insertion of 6 amino acids at the 3′ end of the second zinc finger domain of EVI1. Expression of this EVI1 splice variant enhanced the self-renewal of hematopoietic stem cells, and introduction of mutant SF3B1 in mice bearing the humanized inv(3)(q21q26) allele resulted in generation of this novel EVI1 isoform in mice and hastened leukemogenesis in vivo. The mutant SF3B1 spliceosome depends upon an exonic splicing enhancer within *EVI1* exon 13 to promote usage of a cryptic branch point and aberrant 3′ splice site within intron 12 resulting in the generation of this isoform. These data provide a mechanistic basis for the frequent cooccurrence of *SF3B1* mutations as well as new insights into the pathogenesis of myeloid leukemias harboring inv(3)/t(3;3).

Introduction

Acute myeloid leukemia (AML) with inv(3)(q21q26) or t(3;3)(q21q26) is recognized by the World Health Organization as a unique subtype of AML (henceforth referred to as "inv(3)/t(3;3) AML"),[1] which has a dismal median overall survival (OS) of <1 year after diagnosis.[2-5] This same genomic alteration is also occasionally encountered in patients with myelodysplastic syndromes (MDS), where it is similarly associated with short survival.[4,6] Given the poor outcome of inv(3)/t(3;3) MDS/AML, there have been extensive efforts to dissect the genomic and epigenomic events that give rise to this aggressive disease. Recent efforts have identified that inv(3)/t(3;3) chromosomal rearrangements reposition the *GATA2* enhancer from its normal location at 3q21 to drive ectopic expression of the *EVI1* proto-oncogene from within *MDS1 and EVI1 complex locus* (*MECOM*) at 3q26 (supplemental Figure 1A, available on the *Blood* Web site). Intergenic splicing of *MDS1* and *EVI1* normally results in expression of an *MDS1-EVI1* transcript from *MECOM*, but in patients

with inv(3)/t(3;3) chromosomal alterations, the full-length *MDS1-EVI1* transcript is no longer expressed, and there is monoallelic expression of *GATA2*.[7,8]

EVI1 encodes a transcription factor that is indispensable for hematopoiesis and contains 2 zinc finger (ZF) DNA binding domains, one at the N-terminus and the other at the protein's C-terminus, which includes 7 and 3 ZFs, respectively. In contrast to our understanding of the pathogenic consequences of inv(3)/t(3;3) chromosomal rearrangements, the role of genomic alterations coexisting with inv(3)/t(3;3) is less well understood. For example, monosomy 7 and mutations in *RUNX1*, *IKZF1*, and RAS pathway genes (*NRAS*, *KRAS*, *PTPN11*, and *NF1*)[5,9-11] are known to occur in inv(3)/t(3;3) AML. However, the specific contribution of additional genomic events to inv(3)/t(3;3) leukemia is not clear.

Here, we identify that mutations in the core RNA splicing factor *SF3B1* are the most common coexisting genetic alterations among patients with inv(3)/t(3;3) MDS and AML. Introduction of mutant SF3B1 in mice bearing the humanized inv(3)(q21q26) allele hastened leukemogenesis. Surprisingly, mutant SF3B1 resulted in the generation of a novel isoform of *EVI1*, which alters its second ZF domain and promotes oncogenicity in vivo. This particular oncogenic EVI1 isoform is an unannotated novel transcript and is expressed in nearly one-third of patients with inv(3)/t(3;3) MDS and AML. These data thereby elucidate a mechanistic basis for the frequent cooccurrence of *SF3B1* mutations in inv(3)/t(3;3) leukemias, identify a novel previously unknown oncogenic form of *EVI1*, and delineate a role for pathologic splicing in inv(3)/t(3;3) AML.

Methods

Patient samples

Studies were also approved by the institutional review boards of Memorial Sloan Kettering Cancer Center (MSKCC) and The Medical Ethical Committee of the Erasmus MC and conducted in accordance with the Declaration of Helsinki protocol. Informed consents were obtained from all human subjects. Next-generation sequencing was performed on DNA extracted from bone marrow (BM) mononuclear cells and matched normal from fingernails. Patient samples were sequenced with MSK-IMPACT targeted sequencing panel, with somatic mutations (substitutions and small insertions and deletions), gene-level focal copy number alterations, and structural rearrangements detected with a clinically validated pipeline as previously described.[12,13] All patients with myeloid neoplasms (AML, MDS, chronic myelomonocytic leukemia, and blast-phase chronic myeloid leukemia) and inv(3)/t(3;3) were identified from the electronic medical record and included in this study if next-generation sequencing data were available.

Animals

All animals were housed at MSKCC and at Foundation for Biomedical Research and Innovation (FBRI, Japan) using a 12-hour light/12-hour dark cycle and with ambient temperature maintained at 72°F ± 2°F (~21.5°C ± 1°C) with 30% to 70% humidity. All animal procedures were completed in accordance with the Guidelines for the Care and Use of Laboratory Animals and were approved by the Institutional Animal Care and Use Committees at MSKCC and FBRI. All mouse experiments were performed in accordance with a protocol approved by the MSKCC (11-12-029) and FBRI (18-06) Institutional Animal Care and Use Committee. *Mx1*-Cre and *Sf3b1*^{K700E} mice were obtained from The Jackson Laboratory and were previously generated, respectively.[14] inv(3)(3q21q26) mouse strain (RBRC09508) was provided by RIKEN BRC through the National BioResource Project of the MEXT/AMED, Japan.[7] All of the primers and polymerase chain reaction (PCR) conditions are listed in supplemental Table 1.

Cell lines and tissue culture

HEK293T and PlatE cells were obtained from American Type Culture Collection (Manassas, VA) and Toshio Kitamura (University of Tokyo) and cultured in Dulbecco's modified Eagle medium with 10% fetal bovine serum (FBS). K562, MEL270, MOLM-1, Kasumi-3, HNT-34, and 5637 cells were cultured in RPMI 1640 with 10% FBS. Kasumi-4 cells were cultured in RPMI 1640 with 20% FBS and 10 ng/mL granulocyte-macrophage colony-stimulating factor (AF-300-03, PeproTech). YCU-AML1 cells were cultured with OP-9 in Iscove's modified Dulbecco's medium with 10% FBS, 55 μM β-mercaptoethanol (Sigma-Aldrich) and 20 ng/mL granulocyte-macrophage colony-stimulating factor (PeproTech). MUTZ-3 cells were cultured in α minimum essential medium (with ribo- and deoxyribonucleosides)/20% FBS and 20% conditioned medium of cell line 5637. All cell culture media include 100 U/mL penicillin and 100 μg/mL streptomycin (Gibco).

EVI1 minigene assay

K562 parental and K562-*SF3B1*$^{K666N/WT}$ cells were seeded into a 12-well plate with culture medium 48 hours before transfection of minigene constructs (more details are provided in supplemental methods) in the presence of X-tremeGENE HP DNA transfection reagent (Roche) according to the manufacturer's directions. Forty-eight hours after transfection, cells were collected, and RNA was extracted using RNeasy mini kit (Qiagen). Extracted RNA was treated with DNase I (Ambion) to ensure complete removal of DNA. Minigene-derived and endogenous *EVI1* transcripts were analyzed by reverse transcription (RT)-PCR using specific primers (supplemental Table 1).

Results

SF3B1 mutations are frequent within inv(3)/t(3;3) AML

Prior genomic analyses of cohorts of patients with inv(3)/t(3;3) myeloid neoplasm identified a number of genomic rearrangements coexisting with inv(3)/t(3;3) rearrangement.[10,11] To further evaluate the landscape of genomic alterations within inv(3)/t(3;3) myeloid neoplasms, we compiled prior cohorts of genomic analysis of patients with inv(3)/t(3;3) myeloid neoplasm (n = 63 patients from the Dutch-Belgian Cooperative Trial Group for Hematology-Oncology/the German-Austrian AML Study Group, Leucegene, and BeatAML)[10,11,15] with a previously unpublished cohort of 46 patients with inv(3)/t(3;3) myeloid neoplasm (supplemental Table 2). Interestingly, this revealed that the single most commonly mutated gene in patients with inv(3)/t(3;3) myeloid neoplasm was the core RNA splicing factor *SF3B1* (Figure 1A), although RAS pathway mutations (*NRAS*, *PTPN11*, *KRAS*, and *NF1*) as a group in aggregate (present in 63 out of 109 patients [57.8%]) are more frequent than mutations in

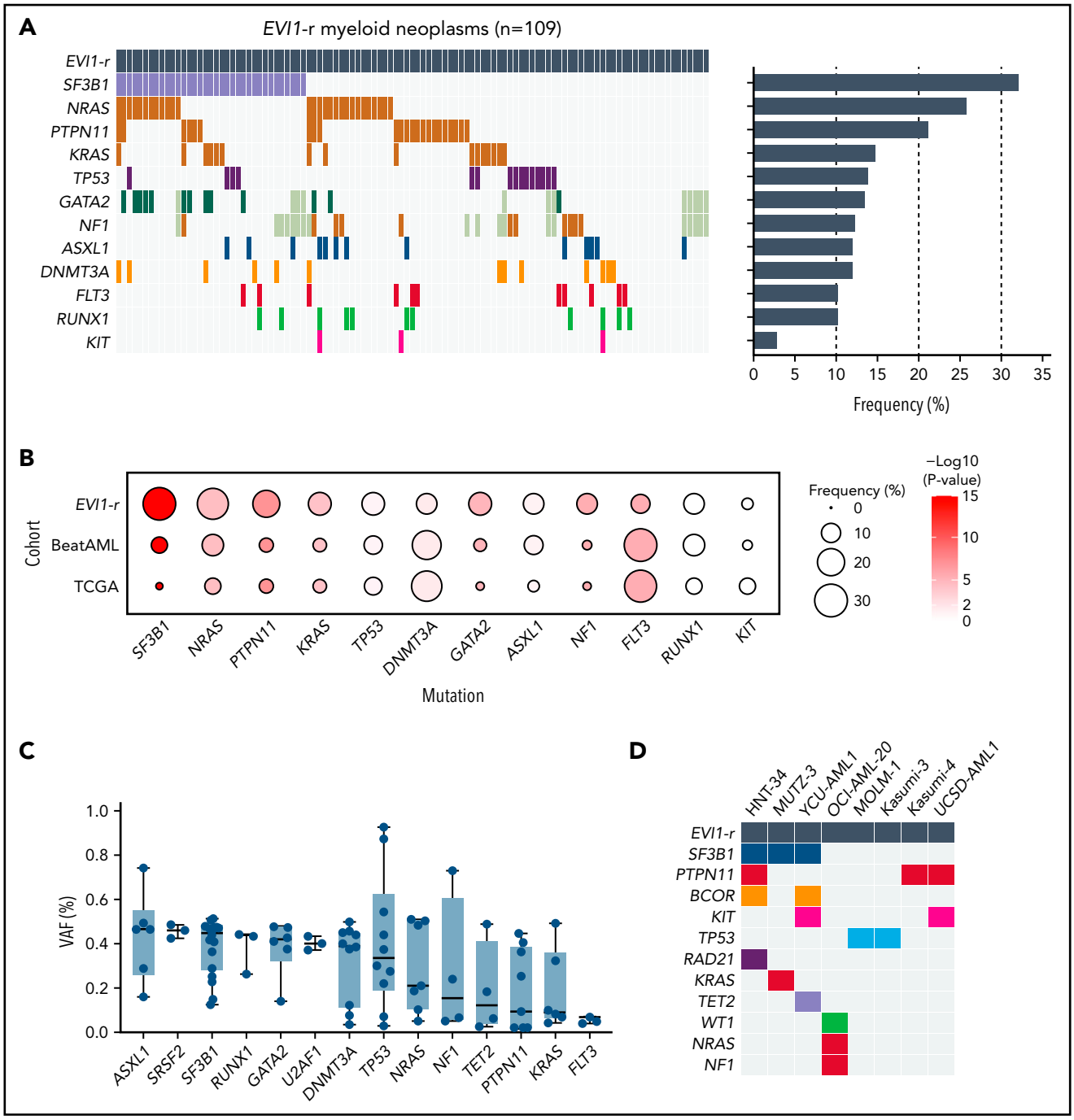

Figure 1. Frequent cooccurrence of *SF3B1* mutations in myeloid malignancies with inv(3)(q21q26) or t(3;3)(q21q26). (A) Oncoprint of recurrently mutated genes in 109 patients with *EVI1*-rearranged (*EVI1*-r) myeloid neoplasms. Horizontal bars show the mutational frequency of each gene. Gray color indicates data not available. (B) Frequency (indicated by bubble size) and statistical enrichment (indicated by color gradient) of mutations (x-axis) across AML (y-axis; inv(3)/t(3;3) patients from panel A, n = 109; BeatAML study, n = 622; TCGA AML study, n = 200). *P* values of Fisher's exact test are color-coded. (C) VAF of mutations in *SF3B1* and *RAS*-associated genes relative to mutations in transcriptional factors, chromatin modifiers, RNA splicing factors in patients with *EVI1*-r myeloid neoplasm. (D) Oncoprint of recurrently mutated genes in *EVI1*-r leukemia cell lines.

SF3B1. *SF3B1* mutations were present in 32.1% of patients and located at hotspot residues in HEAT repeat domains, such as K700 and K666 (supplemental Figure 1B).[16,17] In contrast to the high frequency of mutations in *SF3B1* within *EVI1*-rearranged myeloid neoplasms, mutations in *SRSF2* or *U2AF1* were not uniquely enriched among *EVI1*-rearranged AML combined with overall patients with AML from TCGA/BeatAML cohorts (6.52% vs 8.03% in *SRSF2* mutation [*P* = .6126], 6.52% vs 4.33% [*P* = .4485] in *U2AF1* mutation).[15,18] RNA splicing factor mutations were mutually exclusive in our MSKCC cohort except for 1 patient harboring *SF3B1*-K666R (variant allele frequencies [VAFs] = 47.1%) and *SRSF2*-P95H (VAF = 42.4%).

This high frequency of *SF3B1* mutations within inv(3)/t(3;3) AML was particularly conspicuous because *SF3B1* mutations are most commonly enriched in patients with myeloid leukemia with MDS

with ringed sideroblasts (MDS-RS) (65%-81%),[16,17,19-21] whereas they are relatively rare in AML (~4%).[22] Indeed, compared with mutational analyses of AML cohorts without chromosome 3 alterations,[15,18] inv(3)/t(3;3) AML was characterized by a remarkably higher rate of mutations in *SF3B1* ($P = 1.16 \times 10^{-17}$), RAS-associated pathway genes, and *GATA2*. On the other hand, *EVI1*-rearranged (*EVI1*-r) AML exhibited lower rates of mutations in *FLT3* and *DNMT3A*, when compared with AML without *EVI1*-r (Figure 1B). In contrast to RAS-associated pathway mutations, *SF3B1* mutations tended to contribute to the founder clones in most patients with *SF3B1*-mutated *EVI1*-r myeloid based on the relative VAFs (median VAF of *SF3B1* mutations in inv(3)/t(3;3) samples was 0.448) (Figure 1C). Interestingly, across all inv(3)/t(3;3) human AML cell lines (HNT-34, Kasumi-3, Kasumi-4, MOLM-1, MUTZ-3, OCI-AML20, and UCSD-AML1, and YCU-AML1), 3 of 8 of these lines contain a well-described heterozygous *SF3B1* hotspot mutation (Figure 1D; supplemental Tables 3 and 4). In fact, these 3 cell lines (HNT-34, MUTZ-3, and YCU-AML1) represent the only known AML cell lines with naturally occurring *SF3B1* mutations. Moreover, in the analysis of correlations across all pairwise combinations among 12 frequently mutated drivers, inv(3)/t(3;3) AML exhibited a distinct pattern of positive and negative correlations relative to that in patients with whole MDS/AML (supplemental Figure 1C).[23] For example, *SF3B1* is significantly comutated with *GATA2* within inv(3)/t(3;3) myeloid neoplasms, whereas this correlation was not detected in wider MDS/AML cohorts.[23] These results highlight a unique enrichment of *SF3B1* mutations in inv(3)/t(3;3) AML compared with other AML subtypes. In our MSKCC cohort, we found no significant difference between *SF3B1*-mutated and wild-type (WT) patients in OS from the time of inv(3)/t(3;3) detection (188 vs 179 days; hazard ratio 0.83 [0.41-1.69]). Moreover, OS from the time of initial disease diagnosis was comparable (520 vs 366 days; hazard ratio 0.63 [0.31-1.27]) (supplemental Figure 1D).

SF3B1 mutations promote leukemogenicity in humanized inv(3)(q21q26) mice

Given the recurrent nature of *SF3B1* mutations in inv(3)/t(3;3) AML, we hypothesized that spliceosomal alterations are important in the development of inv(3)/t(3;3) myeloid malignancies. We therefore set out to test this hypothesis by generating a mouse model permitting time- and tissue-specific induction of mutant *Sf3b1* in the presence of the human inv(3)(q21q26) allele. This was accomplished by generating *Mx1*-Cre *Sf3b1*$^{K700E/WT}$ inv(3)(q21q26) mice (along with single-mutant and WT control mice; Figure 2A). We used transgenic mice harboring a human bacterial artificial chromosome encompassing the human inv(3)(q21q26) allele[7] (hereafter referred to as "inv(3) mice") (supplemental Figure 1A) and crossed these animals to mice with conditional knock-in of mutant *Sf3b1* K700E.[14] We thereby generated animals with 4 different genotypes: *Mx1*-Cre control, *Mx1*-Cre inv(3), *Mx1*-Cre *Sf3b1*$^{K700E/WT}$, and *Mx1*-Cre inv(3) *Sf3b1*$^{K700E/WT}$.

We first evaluated the impact of mutant SF3B1 on the clonogenic capacity of inv(3)(q21q26) hematopoietic cells. We collected whole BM cells 4 weeks after polyinosinic-polycytidylic acid (pIpC) injection and evaluated colony formation in methylcellulose media optimized for each hematopoietic lineage (Figure 2B). Hematopoietic cells from either *Mx1*-Cre inv(3) or *Mx1*-Cre inv(3) *Sf3b1*$^{K700E/WT}$ mice produced virtually no BFU-E erythroid progenitor or pre-B lymphoid progenitor colonies (supplemental Figure 2A). In contrast, these BM cells enhanced the clonogenic capacity of myeloid progenitors. Although both were replatable into the fifth round, *Mx1*-Cre inv(3) *Sf3b1*$^{K700E/WT}$ produced more colonies in the second and fifth platings than inv(3) mice alone.

We next evaluated the cell-autonomous effects of hematopoietic stem cells from each mouse model by performing BM transplantation assays into lethally irradiated CD45.1 recipient mice (Figure 2A). After confirming successful engraftment, we treated recipient mice with pIpC 4 weeks after transplantation. Interestingly, inv(3) *Sf3b1*$^{K700E/WT}$ double-mutant mice exhibited significant leukopenia and macrocytic anemia compared with either mutation alone (Figure 2C; supplemental Figure 2B). However, 6 months after pIpC injection, hematopoietic stem and progenitor cell (HSPC) fractions, including LSK ($Lin^-c\text{-}Kit^+Sca1^+$), multipotent progenitors 2/3 (MPP2/3; $CD135^-CD150^+CD48^+$LSK and $CD135^-CD150^-CD48^+$LSK, respectively), and common myeloid progenitors ($Lin^-c\text{-}Kit^+Sca1^-CD34^+Fc\gamma R^-$) (Figure 2D-E; supplemental Figure 2C), were significantly expanded in the double-mutant model, suggesting ineffective hematopoiesis. In the peripheral blood, myeloid-lineage skewing was observed at the expense of B-cell commitment, which was most significant in inv(3)/Sf3b1 double-mutant mice (Figure 2F). In addition to splenomegaly, histological and morphological analysis of BM and spleen cells in the double-mutant mice revealed hypercellularity, destruction of normal architecture, morphological abnormalities, and frequent immature blasts with slight differentiation toward myeloid lineage (Figure 2G; supplemental Figure 3). As a result, *Mx1*-Cre inv(3) *Sf3b1*$^{K700E/WT}$ mice had hastened death owing to MDS and AML (supplemental Figure 2D-E) even when compared with *Mx1*-Cre inv(3) ($P = .0389$) (Figure 2H). Moreover, serial transplantation of double-mutant mouse cells led to more rapidly lethal leukemia vs inv(3) leukemia cells alone (Figure 2I). These results indicate that the *SF3B1* mutation enhanced and accelerated inv(3)-associated myeloid malignancies in a genetically accurate murine model.

Inv(3) rescues the fitness disadvantage of *SF3B1*-mutated HSPCs

A series of studies reported significantly lower peripheral blood chimerism derived from *Sf3b1*$^{K700E/WT}$ mouse hematopoietic precursors in competitive transplantation,[14,24] suggesting that *SF3B1* mutations impair cell-autonomous repopulating when present alone. We therefore evaluated the in vivo self-renewal of *Mx1*-Cre control, *Mx1*-Cre inv(3), *Mx1*-Cre *Sf3b1*$^{K700E/WT}$, and *Mx1*-Cre inv(3) *Sf3b1*$^{K700E/WT}$ models by performing BM competitive transplantation assays. Equal numbers of $CD45.2^+$ BM cells from each of these models were mixed with $CD45.1^+$ WT BM cells and injected into lethally irradiated CD45.1 recipient mice (supplemental Figure 4A). Five months later, whole BM cells of each group were serially transplanted into new $CD45.1^+$ recipient mice to determine the further reconstitution capacity. Interestingly, in stark contrast to the near-complete loss of hematopoiesis in *Mx1*-Cre *Sf3b1*$^{K700E/WT}$ mice, the inv(3) transgene rescued the impaired in vivo clonogenic capacity of *Sf3b1*-mutated HSPCs, especially in secondary transplant (supplemental Figure 4B). This was associated with rescued chimerism of myeloid-lineage cells in the BM as well as stem and progenitor cells in BM 5 months following primary

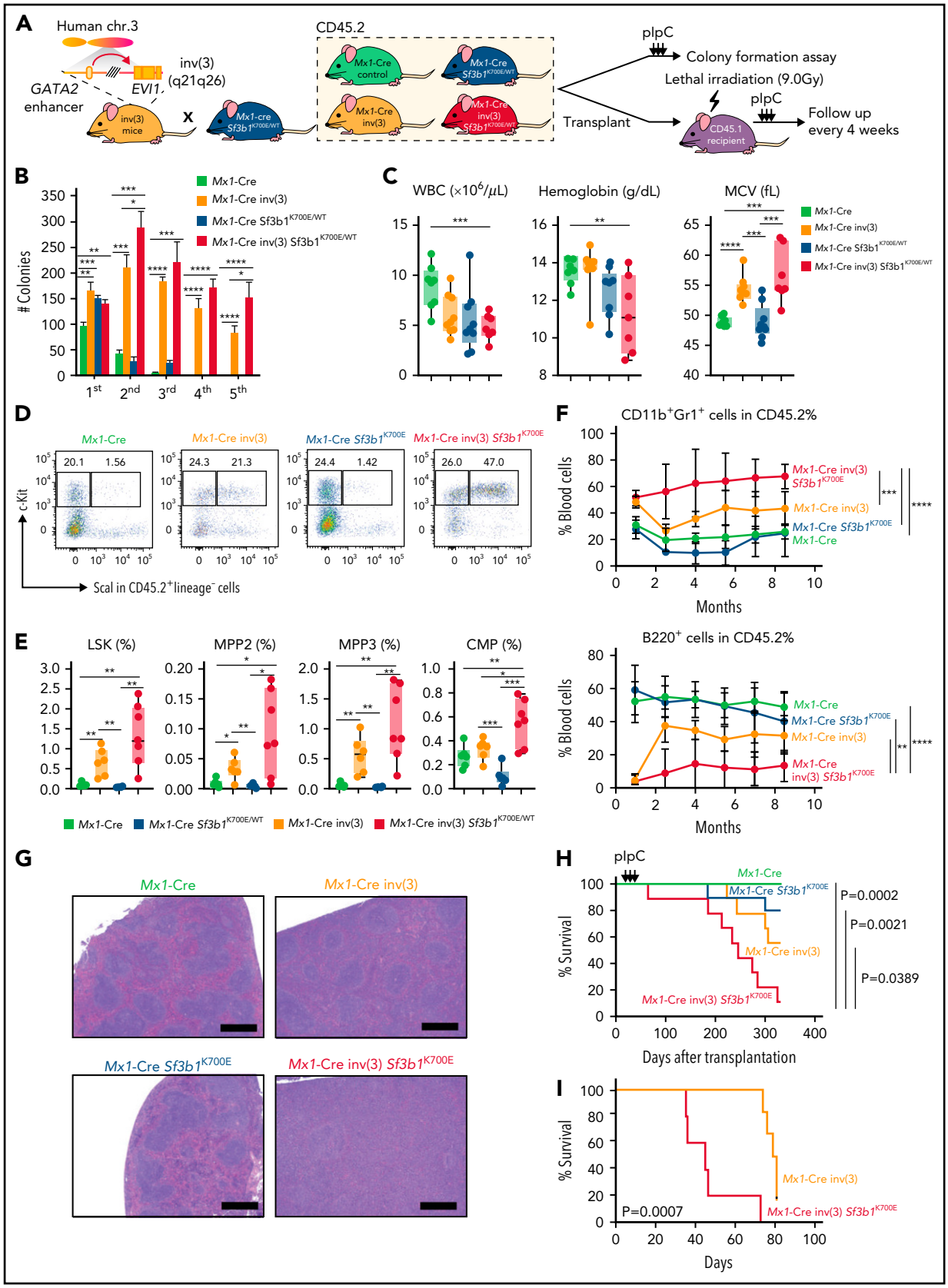

Figure 2.

transplantation. In line with the results of in vitro colony-forming assay, no rescue was observed in B220$^+$ cells (supplemental Figure 4C-D).

Transcriptome analysis of SF3B1 mutant/inv(3) HSPCs

We next performed RNA-seq analyses of mouse and human leukemias to identify the impact of inv(3) and *SF3B1* mutations alone and together on splicing and gene expression. RNA-seq analysis of fluorescence-activated cell sorter–purified lineage-negative c-Kit$^+$ cells of the mouse models described above was performed 2 months after pIpC injection, in biological triplicate for each model. Unsupervised hierarchical clustering analysis, using Euclidean distance and Complete linkage method, revealed that transcriptomes of lineage-negative c-Kit$^+$ cells from *Mx1*-Cre inv(3) and *Mx1*-Cre inv(3) *Sf3b1*$^{K700E/WT}$ groups differed substantially from *Mx1*-Cre control and *Mx1*-Cre *Sf3b1*$^{K700E/WT}$ groups, suggesting potent gene expression effects of the inv(3) transgene (Figure 3A). Similarly, principal component (PC) analysis revealed differences in the transcriptome of *Mx1*-Cre inv(3) and *Mx1*-Cre inv(3) *Sf3b1*$^{K700E/WT}$ groups vs *Mx1*-Cre control *Mx1*-Cre *Sf3b1*$^{K700E/WT}$ groups. PC1 accounted for 65% of the variance and defined the presence of the inv(3) transgene (Figure 3B). At the same time, PC2 clearly distinguished *Mx1*-Cre inv(3) *Sf3b1*$^{K700E/WT}$ from *Mx1*-Cre inv(3), indicating that Sf3b1 mutant exerted additive gene expression effects on inv(3) HSPCs, which is consistent with the collaborative biological outcomes of double-mutant mice described above (Figure 2).

Differential gene expression analysis identified 6659, 2609, and 6796 genes dysregulated compared with control (Student *t* test, $P < .01$; fold change >2 or <0.5) in inv(3), *Sf3b1*$^{K700E/WT}$, inv(3) *Sf3b1*$^{K700E/WT}$ mice, respectively. Interestingly, a large portion of differentially expressed genes in the inv(3) *Sf3b1*$^{K700E/WT}$ group were shared with those of the inv(3) group rather than the *Sf3b1*$^{K700E/WT}$ group (65.9%, 4481/6796 genes vs 22.3%, 1514/6796 genes) (Figure 3C). We identified significant enrichment for Gene Ontology (GO) and pathway terms reflecting the development of MDS/AML in inv(3)/Sf3b1 double-mutant mice, including MAP kinase, interferon, tumor necrosis factor-α, and NF-κB signaling as well as interleukin-6 activation (Figure 3D; supplemental Figure 5). Consistent with the results in Figure 3C, the dysregulated pathways and GO terms were mainly attributed to the effect of inv(3), especially in upregulated pathways (Figure 3D; supplemental Figure 5A).

In order to evaluate these findings in patient samples, we analyzed RNA-seq data of unfractionated BM mononuclear cells isolated from 7 *SF3B1*-mutant/*EVI1*-r, 5 *SF3B1*-WT/*EVI1*-r, 2 *SF3B1*-mutant, and 7 *SF3B1*-WT normal karyotype AML patient samples. In line with the mouse RNA-seq results (Figure 3C-D), in the presence of the *EVI1*-r, the *SF3B1* mutation had limited impact on gene expression in terms of dysregulated pathways evaluated by using GO enrichment terms in the algorithm of Enrichr (https://maayanlab.cloud/Enrichr/) (Figure 3E). As such, a large proportion of differentially expressed genes in the *SF3B1*-mutant/*EVI1*-r group overlapped with those of the *SF3B1*-WT/*EVI1*-r patient samples (Figure 3E).

We next sought to identify aberrant splicing events associated with *SF3B1* mutation and *EVI1*-r. Of note, the number of aberrantly spliced genes was largest in *SF3B1*-mutant/inv(3) patient samples where the majority of splicing changes could be attributed to the presence of the *SF3B1* mutation (Figure 3F). Consistent with previous studies,[25,26] aberrant 3′ splice site (3′ss) usage was the most prevalent mis-splicing event in the *SF3B1*-mutant/inv(3) group (Figure 3G), although such effects were relatively modest in murine models (supplemental Figure 5B). These transcriptome analyses suggested cooperative effects of the *SF3B1* mutation and inv(3) allele on aberrant splicing and gene expression, respectively.

EVI1 mis-splicing in *SF3B1*-mutant cells

As noted in prior studies,[24,27,28] despite striking similarities in global aberrant splicing patterns induced by SF3B1 mutants across diverse species, there was modest overlap in aberrantly spliced events in mouse vs human cells. Interestingly, however, we identified that human *EVI1* itself was recurrently targeted in human *SF3B1*-mutant/inv(3) patient samples (Figure 4A).

Intriguingly, the *SF3B1* mutation was associated with aberrant 3′ss selection at the intron 12-exon 13 junction of *EVI1* (NM_001105078.4), which encodes the C-terminal end of the second ZF domain of EVI1. EVI1 contains 10 ZFs that are arranged in 2 separate domains, each of which binds different consensus DNA sequences (Figure 4A).[29] This *EVI1* mis-splicing event was exclusively observed in *SF3B1*-mutant myeloid malignancy patient samples and cell lines and present across *SF3B1* hotspot mutations (Figure 4B; supplemental Table 5). For example, the inv(3)/t(3;3) AML cell lines HNT-34 and YCU-AML1 harboring *SF3B1*K700E heavily express this variant *EVI1* isoform (Figure 4C).[30,31] Expression of several *SF3B1* mutations (K700E, K666N, and G740E), but not WT *SF3B1*, into K562 cells similarly resulted in the aberrant *EVI1* isoform generation (supplemental Figure 6A). Sanger sequencing of this isoform verified that this splice variant results in the introduction of 18 nucleotides inserted between exons 12 and 13 of the *EVI1* transcript, at the very 3′ end of intron 12 (Figure 4D). This nucleotide insertion gives rise to an in-frame insertion of 6 amino acids (FLLHTG) (Figure 4D). This exact same +18 *EVI* splice variant was

Figure 2. *SF3B1* mutations enhance the leukemogenicity of hematopoietic cells expressing the inv(3)(q21q26) allele. (A) Schema of generation of CD45.2 *Mx1*-cre inv(3) *Sf3b1*$^{K700E/WT}$ mice (left) and schema of in vitro and in vivo analyses of hematopoiesis from these mice and single-mutant controls. (B) Number of myeloid colonies on first to fifth plating of *Mx1*-cre inv(3) *Sf3b1*$^{K700E/WT}$ mice and controls. (C) Box-and-whisker plots of white blood cell count (WBC), hemoglobin, and mean corpuscular volume (MCV) from CD45.1 recipient mice following 8.5 months of transplantation of CD45.2 mice from panel A. For box-and-whiskers plots throughout, bar indicates median, box edges first and third quartile values, and whisker edges minimum and maximum values. (D) Representative fluorescence-activated cell sorter plots of CD45.2$^+$ LSK (lineage-negative Sca1$^+$ and c-Kit$^+$) and LK (lineage-negative Sca1$^-$ and c-Kit$^+$) cells from BM of CD45.1 recipient mice at 4 months posttransplant. % of cells within gate is shown. (E) Box-and-whisker plots of percentage of BM CD45.2$^+$ LSK, multipotent progenitor cells 2 and 3 (MPP2 and MPP3, respectively), and common myeloid progenitor (CMP) cells. (F) % of CD11b$^+$Gr1$^+$ and B220$^+$ cells among CD45.2$^+$ cells in peripheral blood over time following transplantation. Mean ± standard deviation are shown. (G) Representative hematoxylin-and-eosin stain (original magnification ×100) of spleen of CD45.1 primary recipient mice. Scale bars, 400 μm. (H) Kaplan-Meier survival curve of primary CD45.1 recipient mice. *P* values were calculated by log-rank test. (I) Kaplan-Meier survival curve of secondarily transplanted CD45.1 recipient mice following sublethal irradiation (4.5 Gy). *P* values were calculated by 2-sided Student *t* test or log-rank test. *$P < .05$, **$P < .01$, ***$P < .001$, and ****$P < .0001$. chr., chromosome.

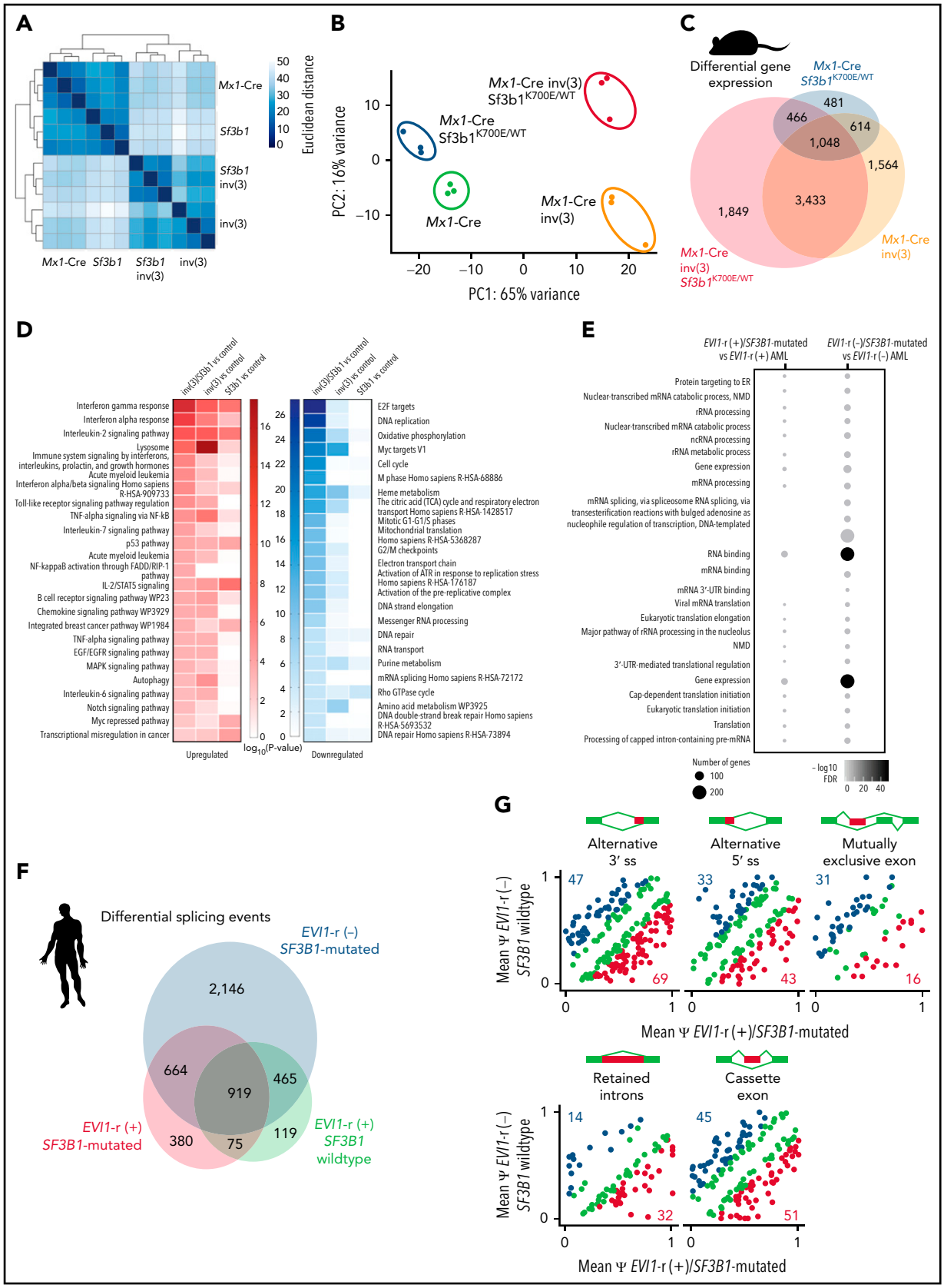

Figure 3.

expressed in *Mx1*-Cre inv(3) *Sf3b1*$^{K700E/WT}$ double-mutant mice, indicating that murine Sf3b1 mutant similarly induces aberrant 3′ss selection of human *EVI1* contained within the bacterial artificial chromosome transgene recapitulating the inv(3)(q21q26) allele (Figure 4E; supplemental Figure 6B). Interestingly, a model structure by AlphaFold2,[32] which predicts 3-dimensional protein structure from amino acid sequence using a deep learning system, revealed that the EVI1 + 18 splicing event introduces 6 amino acids immediately after the second ZF domain of EVI1 (supplemental Figure 6C). This change in protein sequence may alter DNA recognition by the second ZF domain. Hereafter, the newly discovered *EVI1* (*MECOM*) splice variant will be referred to as "*EVI1*+18."

Functional impact of the novel *EVI1*+18 splice variant

We next sought to understand the biological effects of the aberrant +18 isoform and generated a pMYs-IRES-GFP retrovirus vector to express WT *EVI1* (NM_001105078.4, EVI1-145 kDa) or *EVI1*+18 cDNA. Several studies have demonstrated that ectopic *EVI1* expression in hematopoietic stem cells leads to increased colony output and immortalization in methylcellulose media,[33] which was confirmed by our experiments. Interestingly, however, *EVI1*+18 further enhanced proliferation capacity compared with WT *EVI1* in colony formation assay (Figure 4F). We performed RNA-seq analysis of the fourth colonies and validated the dysregulated genes by quantitative RT-PCR. This revealed prominent upregulation of *Hes1*, *Meis1*, *Bcl11a*, and *Cd34* in cells expressing the *EVI1*+18 isoform (supplemental Figure 6D). In addition, we observed a competitive advantage of *EVI1*+18 expressing HSPCs over WT *EVI1*-transduced HSPCs (supplemental Figure 6E-F). Consistent with these data, gene set enrichment analysis demonstrated that genes upregulated in leukemic stem cells are enriched in *EVI1*+18 transduced K562 cells compared with the *EVI1* WT-expressing cells (supplemental Figure 6G). These results indicate that SF3B1-mutants generate a previously unknown *EVI1* variant with enhanced self-renewal capacity.

To test if *EVI1*-r/*SF3B1*-mutated AML cells depend on the aberrant splicing machinery, we evaluated the 50% inhibitory concentration of *EVI1*-r cells with or without *SF3B1* mutation to indisulam, a selective degrader of the RNA splicing factor RBM39.[34] Of note, 3-day dose-response experiments revealed that HNT-34 and MUTZ-3, both of which harbor *SF3B1*^{K700E}/*EVI1*r, were sensitive to indisulam compared with *SF3B1* WT/*EVI1*-r cell lines, Kasumi-3 and K562 cells with t(3;8),[35] as well as *SF3B1* WT/*EVI1* WT cell lines (K562) (supplemental Figure 7). These data suggest that spliceosomal disruption may be therapeutically effective against *EVI1*-rearranged AML with *SF3B1* mutations.

Given the altered second ZF domain of EVI1 + 18, we next sought to evaluate the genomic distribution and transcriptional effects of this EVI1 isoform compared with the most common annotated EVI1 isoform produced in inv(3) AML. To identify genome-wide binding preferences of EVI1 vs EVI1 + 18, we performed anti-EVI1 chromatin immunoprecipitation (ChIP)-seq using HNT-34 (*SF3B1*^{K700E}/*EVI1*-r), MUTZ-3 (*SF3B1*^{K666N}/*EVI1*-r), and MOLM-1 (*SF3B1* WT/*EVI1*-r) cells, as well as 1 primary *SF3B1*^{K700E}/*EVI1*-r AML patient sample (Figure 4G). Leukemias with concomitant *SF3B1* mutation and *EVI1*-r, but not the *SF3B1* WT/*EVI1*-r cell line, expressed the *EVI1*+18 isoform (Figure 4C). Interestingly, we identified 5698 exclusive *EVI1*+18 peaks in *SF3B1* mutant/*EVI1*-r cell lines but not in MOLM-1 (*SF3B1* WT/*EVI1*-r) cells (supplemental Figure 8A). The majority of such peaks (5206 of 5698 peaks, 91.4%) were also detected in primary *SF3B1*^{K700E}/*EVI1*-r AML cells expressing *EVI1*+18, and nearly all are located at promoters. Of note, transcription factor enrichment analysis identified PU.1 (SPI1) motifs significantly enriched in EVI1 + 18-specific peaks (supplemental Figure 8B). Finally, we visualized these ChIP-seq results at several genes important for leukemic transformation, such as *MEIS1* (Figure 4H; supplemental Figure 8C). Given that expression of *Meis1*, a crucial regulator of leukemogenesis,[36] was remarkably increased in the immortalized colonies with *EVI1*+18 (compared with those with *EVI1* WT; supplemental Figure 6D), we speculate that the link between *EVI1*+18 and oncogenic transcriptional program contributes to leukemia development. We also performed ChIP-seq using exogenously EVI1- vs EVI1 + 18-expressing 293T cells (supplemental Figure 9A). In such a model, the genomic distributions of EVI1 and EVI1 + 18 were not strikingly different (supplemental Figure 9B-E) except for a limited number of regions, indicating that the transcriptional regulation by the endogenous promoter and cellular contexts may be important.

Molecular regulation of aberrant *EVI1* splicing by mutant SF3B1

SF3B1, as part of the U2 small nuclear ribonucleoprotein complex, is responsible for recognition of the intronic branchpoint sequence (BPS), which facilitates 3′ss selection.[16,25] To identify *cis*-acting elements, including BPS, polypyrimidine tract, and exonic splicing enhancers (ESEs), required for *EVI1* aberrant splicing by SF3B1 mutants, we generated a minigene construct containing the mis-spliced intron (intron 12) and flanking exons (exons 12 and 13).[37,38] We then mutagenized a variety of sequences within the minigene and transduced WT and mutant minigenes into *SF3B1* WT and K666N knock-in K562 cells to identify those *cis* elements within *EVI1* essential for aberrant splicing by mutant SF3B1 (Figure 5A). As expected, mutant SF3B1, but not WT SF3B1, induced the *EVI1*+18 variant in both the minigene-derived RNA and the endogenous RNA (Figure 5B). Disruption of the cryptic 3′ss eliminated the *EVI1*+18

Figure 3. Combined impact of mutations in *SF3B1* and inv(3)/t(3;3) on gene expression and RNA splicing. (A) Similarity matrix and hierarchical clustering of 4 groups (*Mx1*-Cre control, *Mx1*-Cre inv(3), *Mx1*-Cre *Sf3b1*$^{K700E/WT}$, and *Mx1*-Cre inv(3) *Sf3b1*$^{K700E/WT}$) by differential gene expression. Three samples were independently collected in each group. (B) Principal component (PC) analysis of gene expression from 12 samples (4 groups, biologically triplicated). (C) Overlap of differentially expressed genes compared with *Mx1*-Cre control. (D) Significantly dysregulated pathways. *P* values are color-coded. (E) Significantly dysregulated pathways. Number of genes and statistical significance ($-\log_{10}$FDR) were shown. The impact of *SF3B1* mutation on gene expression was analyzed under the condition with or without *EVI1* rearrangement. (F) Overlap of differentially spliced genes compared with AML without *SF3B1* mutation or *EVI1* rearrangement. (G) Aberrant splicing detected in AML with *EVI1* rearrangement and *SF3B1* mutations. x-axis and y-axis indicate the percent spliced in (ψ) of each splicing event in the presence/absence of genetic alterations. Alternate splice sites, mutually exclusive exons, retained introns, or cassette exons are shown when $P < .01$. Red and blue dots represent individual splicing events or coding genes that are promoted or repressed in each condition; green dots are shown when the difference in percent spliced is <10%. The number of aberrantly spliced genes is indicated in blue or red.

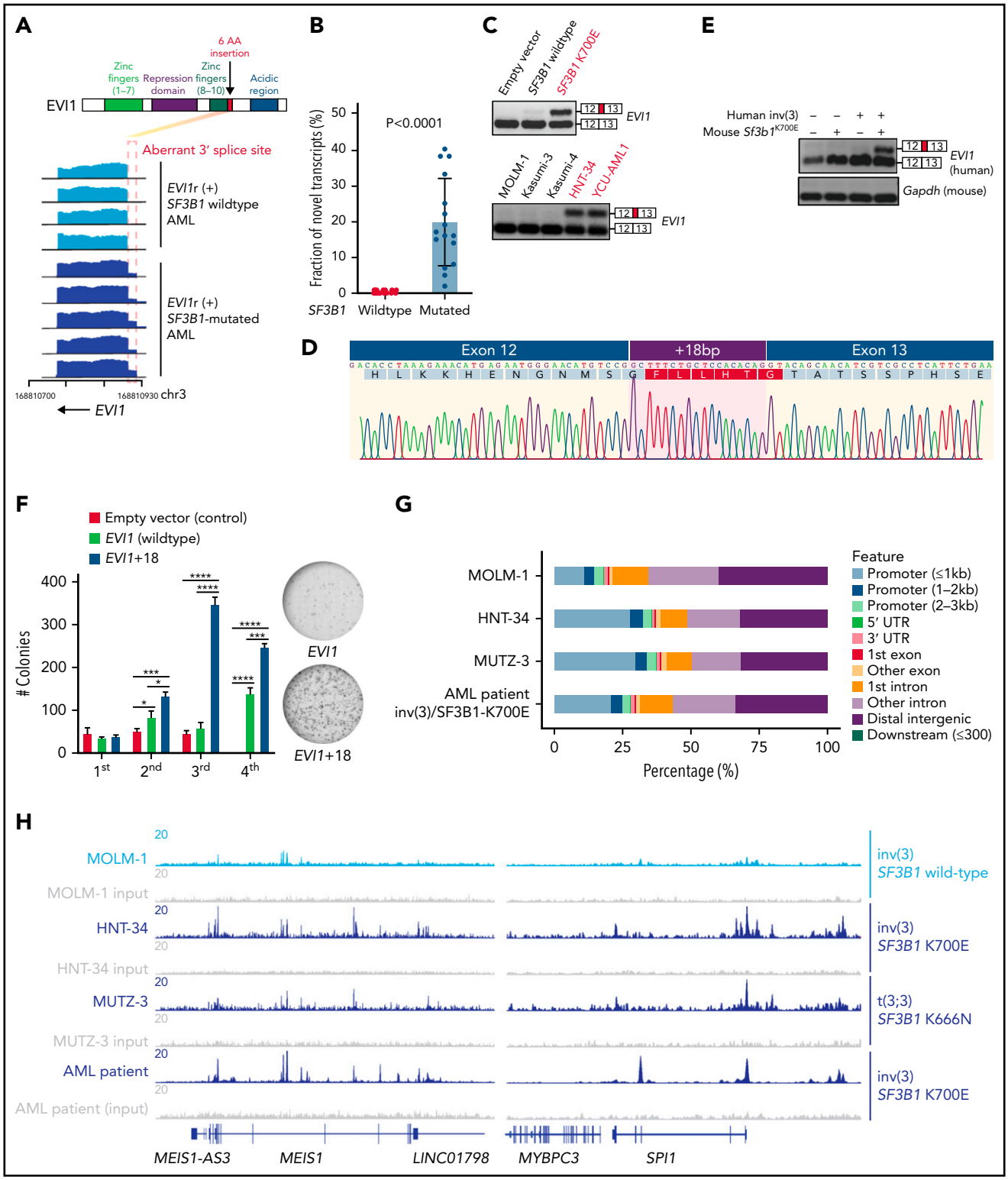

Figure 4. *SF3B1* mutations promote expression of a novel *EVI1* isoform that enhances *EVI1*'s self-renewal capacity. (A) Schematic of EVI1 protein with 6 amino acid insertion (top) and representative RNA-seq coverage plot of *SF3B1* WT and mutated inv(3) AML (bottom). (B) Fraction of the novel transcript (*EVI1*+18) compared with normal transcript in *SF3B1* WT and *SF3B1* mutated *EVI1*-rearranged AML. (C) RT-PCR illustrating the inclusion of intronic sequences in *SF3B1* K700E-transduced MEL270 cells (top, red) and endogenously *SF3B1* K700E harboring leukemia cells (bottom, red). (D) Sanger sequencing of complementary DNA (cDNA) arising from the top band in panel C. The nucleotide sequences and corresponding amino acids are indicated. (E) RT-PCR of human *EVI1* and mouse *Gapdh* using cDNA derived from peripheral blood of 4 murine models. (F) Number of myeloid colonies on first to fourth plating of c-Kit$^+$ BM cells transduced with empty vector (control), *EVI1* (WT), or *EVI1*+18 cDNA (left). Representative images (right) of the sixth colony. (G) Genomic distribution of anti-EVI1 ChIP-seq peaks. (H) Coverage tracks showing EVI1 ChIP-seq occupancy at the indicated genomic loci. *P* values were calculated by 2-sided Student *t* test. **P* < .05, ***P* < .01, ****P* < .001, and *****P* < .0001.

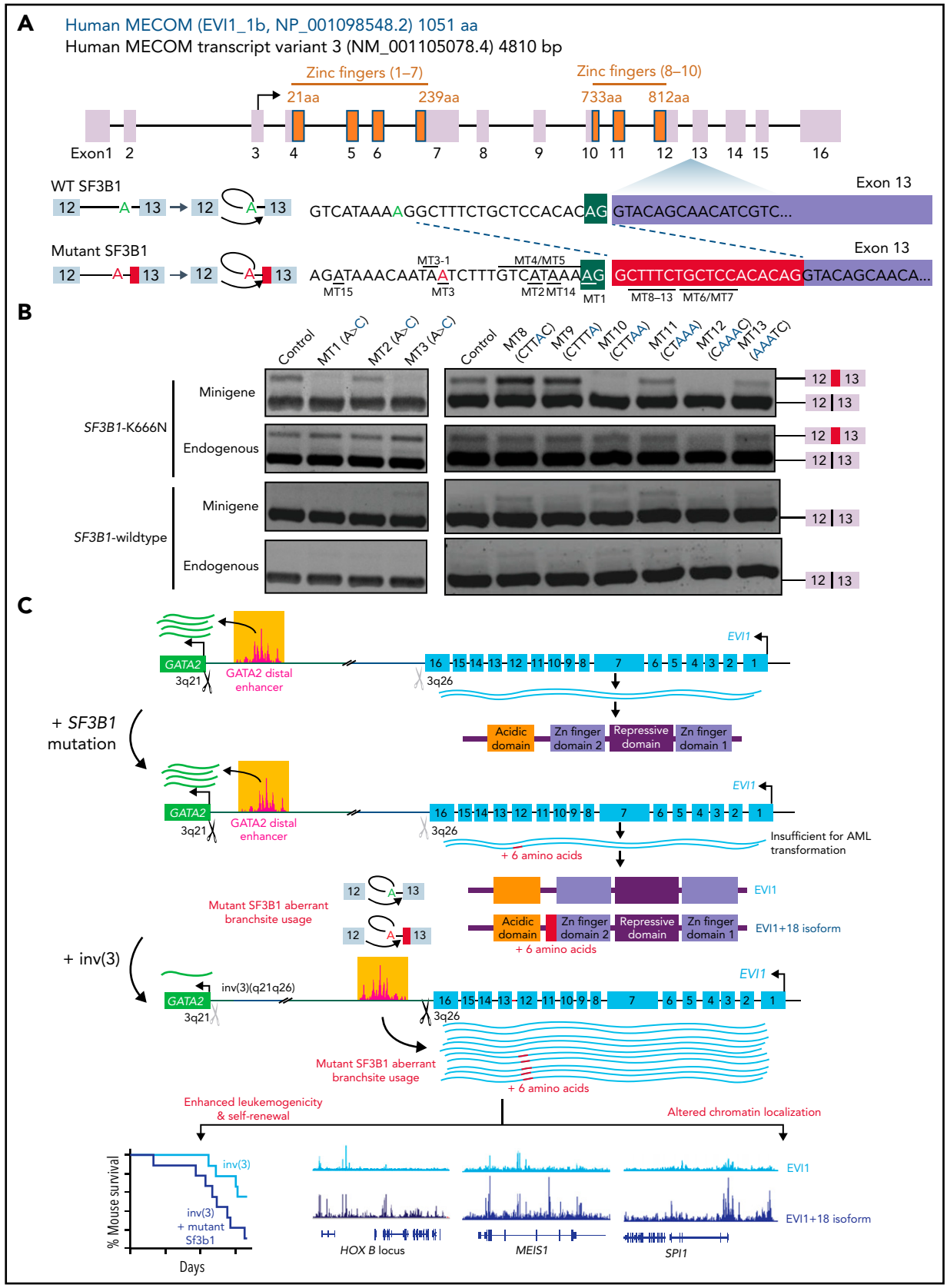

Figure 5.

isoform (this mutant minigene is noted as "MT1"). We then searched for potential cryptic branchpoints used by mutant SF3B1 by mutagenizing 2 adenines upstream of the cryptic 3′ss (MT2 and MT3 minigenes) and concluded that the adenine located at the −16 position upstream of the cryptic 3′ss was indispensable for *EVI1*+18 generation. We mapped branch sites by lariat-sequencing RNA derived from K562 cells with endogenous knock-in of the *SF3B1* K700E mutation (supplemental Figure 10A). We sequenced 6 single colonies to detect branchpoints within this intron and found that the adenosine nucleotides corresponding to the regions at MT1 (3/6), MT2 (1/6), and MT3 (2/6) are used (supplemental Figure 10B). However, it is hard to exclude the possibility that an adjacent adenosine is never used as the branch site because the branchpoint is occasionally deleted or mutated during PCR. Indeed, we found that mutagenesis of the adenosine nucleotide immediately adjacent to MT3 (MT3-1 in Figure 5A, A>C) erased the +18 isoform (supplemental Figure 10C). We next investigated the role of the polypyrimidine tract in generation of this mutant form of *EVI1*. Although a polypyrimidine tract is not consistently observed upstream of an aberrant cryptic 3′ss, the forced introduction of a polypyrimidine tract upstream of the cryptic 3′ss or disruption of the canonical 3′ss's polypyrimidine tract enhanced expression of the *EVI1*+18 by mutant SF3B1 (supplemental Figure 10D, MT4-7). Considering that altering the branchpoint affected generation of the *EVI1*+18 isoform more profoundly than altering the polypyrimidine tract, it is likely that SF3B1 mutants are less dependent on polypyrimidine tract sequences in inducing the aberrant 3′ss selection at this region of *EVI1*. This finding is similar to that seen with mutant SF3B1's of *BRD9* (supplemental Figure 10E).[37]

Next, we sought to identify ESEs necessary for the production of the aberrant *EVI1* transcript by mutant SF3B1. In our prior analyses of *BRD9* mis-splicing by mutant SF3B1, we identified a "TTTCT" sequence as a cryptic ESE within *BRD9* exclusively used by mutant SF3B1.[37] Of note, the *EVI1*+18 variant also contained a "TTTCT" sequence close downstream of the 3′ss. Mutagenizing either 2 or 3 bases around this same sequence within *EVI1* remarkably inhibited the production of *EVI1*+18 (Figure 5B, MT8-13). These results highlight the dependency of SF3B1 mutant-induced mis-splicing of *EVI1* on cryptic BPS selection and a specific ESE. Moreover, we confirmed that AG to AA mutation at the 3′ss completely ablated the normal 3′ss in *SF3B1*-WT condition and promoted usage of the "AG" located at −18 bp upstream as an aberrant 3′ss as observed in *SF3B1* mutated patients (supplemental Figure 10F-G). Finally, because there are annotated single nucleotide polymorphisms (SNPs) (c.2651-23A>G and c.2651-44A>G) near the 3′ss of intron 12 that may affect *EVI1* splicing, we evaluated the impact of these SNPs using our *EVI1* minigene (MT14 and MT15 in Figure 5A, respectively). This revealed that these SNPs modestly affected the splicing in the minigene reporter assay, suggesting that the SNPs in intron 12 may influence the generation of the *EVI1*+18 isoform (supplemental Figure 10G).

Discussion

Although mutations in *SF3B1* are heavily enriched in MDS-RS[21] and there are accumulating data on the impact of *SF3B1* mutations and their consequent mis-splicing in the aberrant erythropoiesis of MDS-RS,[14,24,39,40] specific roles for *SF3B1* mutations in AML are not well explored. Here, we identify a strikingly high frequency of *SF3B1* mutations in adverse myeloid malignancies with inv(3)/t(3;3). Although the pathogenic consequences of how chromosome 3 rearrangements alter the enhancer landscape of *GATA2* and *MECOM* expression have been exquisitely dissected, here we make a novel observation that mutations in *SF3B1* induce aberrant splicing of *EVI1* itself and give rise to a novel oncogenic isoform of *EVI1*.

The splicing event within *EVI1* reported here is distinct from any prior *EVI1* or *MECOM* isoforms described previously. Although there have been extensive prior studies of global splicing alterations as well as individual mis-splicing events induced by mutations in *SF3B1* in a variety of cell and cancer types,[25,26,37,41-44] the current report is the first to report this novel unannotated splicing alteration within *MECOM/EVI1*. Most prior studies have focused on the impact of *SF3B1* mutations on aberrant intron proximal 3′ss usage resulting in out-of-frame transcripts predicted to result in nonsense-mediated messenger RNA (mRNA) decay.[25,26,37] However, this study as well as several important studies on the impact of SF3B1 mutant mis-splicing on aberrant exon inclusion[37] and intron removal[26,44] highlights a diversity of functionally important splicing changes induced by mutant SF3B1.

Although this mis-splicing event in *MECOM/EVI1* is present in *SF3B1* mutant human cells lacking inv(3)/t(3;3) rearrangements, we believe that detection of *EVI1* mis-splicing was facilitated in our studies by the uniquely elevated *EVI1* mRNA expression created by the structural alteration of chromosome 3 studied here (Figure 5C). Although it is clear that expression of this *EVI1*+18 isoform from the endogenous inv(3) allele promoted leukemogenesis in vivo compared with expression of known *EVI1* isoforms from the inv(3) allele, the contribution of the *EVI1*+18

Figure 5. *Cis* elements within *EVI1* required for generation of the *EVI1*+18 bp splice variant by mutant SF3B1. (A) *EVI1* gene structure and protein domains (top). Inset illustrates the transcripts when +18 nucleotides (red rectangle) are excluded (top) or included (bottom). Green A and red A indicate the branchpoint for canonical and aberrant transcripts, respectively. Single underlining indicates sequence motifs that were subsequently mutated in the minigene assay (each individual minigene construct is named "MT1" to "MT13"). aa, amino acid. (B) RT-PCR analysis of the +18 nucleotides inclusion in a minigene (top) or endogenous (bottom) context following transfection of minigenes with the illustrated mutations into *SF3B1*-K666N knocked-in K562 cells and *SF3B1*-WT K562 cells. (C) Schematic of the model proposed by which *EVI1* rearrangements and *SF3B1* mutations promote leukemia development. As previously demonstrated, structural rearrangements at chromosome 3q reposition the *GATA2* distal enhancer to upregulate *EVI1* expression while simultaneously downregulating *GATA2*. As shown in this study, approximately one-third of patients with *EVI1* rearrangements harbor concomitant change-of-function mutations in SF3B1, which promote use of an aberrant intron-proximal branch site within intron 12 of *EVI1*. This splicing alteration generates a stable unannotated transcript of EVI1 ("*EVI1*+18"), which is translated to express an EVI1 protein with insertion of 6 amino acids at the C-terminal end of the second ZF domain of EVI1. The EVI1+18 isoform is expressed whenever any recurrent cancer hotspot mutations in SF3B1 is present in cells with human EVI1 expression. Although EVI1+18 is not sufficient for leukemia transformation on its own, EVI1+18 enhances leukemogenicity in the setting of the EVI1 rearrangement and alters the chromatin localization of EVI1 to loci well known to be involved in leukemia development (such as *MEIS1* and the *HOXB* locus).

isoform in cells without *EVI1* rearrangement remains to be clarified. Although expression of the *EVI1*+18 isoform was seen in every inv(3)/t(3;3) rearranged patient with an *SF3B1* mutation, we witnessed varying levels in the magnitude of expression of this unique *EVI1* isoform.

Currently, it is unclear if the variation in the degree of *EVI1*+18 expression occurred due to differences in allelic frequency of *SF3B1* mutations, the exact SF3B1 mutant residue, potential germline SNPs within *EVI1* intron 12, and/or technical variability owing to leukemia cell purity. Use of emerging long-read RNA-seq technologies may be helpful in illuminating the exact full-length *EVI1* isoforms created in the setting of inv(3)/t(3;3) AML and may even be applied to *EVI1* isoform expression at the single-cell level.[45] It is also possible that structural rearrangements involving the *GATA2* distal enhancer with distinct breakpoints could result in varying levels of *EVI1* upregulation. This point will be important to study in future efforts focusing on cohorts of patients with *EVI1* rearrangements paired with bulk and single-cell genomic data. Moreover, it will be important for future clinical studies involving larger numbers of patients with *EVI1* rearrangements to dissect the clinical impact of coexisting *SF3B1* mutations and presence of distinct *EVI1* isoforms. Finally, given that *SF3B1* mutations are often seen in the setting of clonal hematopoiesis,[46,47] it will be interesting to determine the order of acquisition of *SF3B1* mutations and chromosome 3 structural rearrangements in future studies.

Combined expression of the *SF3B1* mutation with the human inv(3) allele in mice enhanced myeloid lineage skewing, HSPC expansion, and leukemia development, supporting the notion that mutant SF3B1 gives rise to an additional cancer program within inv(3)-inducing leukemia. Evaluation of shared mis-splicing events across human inv(3)/t(3;3) *SF3B1*-mutant AML and our murine models consistently identified this shared *EVI1* mis-splicing event. Importantly, mis-splicing of *EVI1* was only seen in mice when the human *EVI1* sequence was present in mutant SF3B1 mouse cells (as we believe differences in nucleotide sequence between mouse and human intron 12 precluded mis-splicing of mouse *Evi1*). Although our data do not eliminate the possibility that additional mutant SF3B1 mis-splicing events can contribute to inv(3)/t(3;3) leukemogenesis, ectopic expression of this *EVI1*+18 isoform enhanced self-renewal of HSPCs.

Mechanistically, the novel *EVI1*+18 appears to alter chromatin and/or DNA binding relative to WT *EVI1* (Figure 5C). Structural predictions suggest the possibility that the additional 6 amino acids generated by the *EVI1*+18 splicing event may alter the function of the second ZF domain of EVI1.[32] Interestingly, most monoallelic mutations within MECOM in patients with the *MECOM*-associated syndrome patients occur in the second ZF domain and many occur at this same splice site.[48] These observations suggest that mutations or mis-spliced forms of this ZF domain occur in multiple EVI1-associated diseases.

It is hoped future biochemical and structural studies of this *EVI1* isoform will clarify the biophysical impact of the *EVI1*+18 on *EVI1* function in more detail. For example, it is possible that this mis-splicing event or mutations in this domain of EVI1 may disrupt the secondary structure of the second Zn finger domain and/or interfere with zinc coordination. Overall, given the dismal outcome in patients with inv(3)/t(3;3) MDS and AML, the models developed here will be an important resource for future therapeutic and mechanistic studies, and this subtype of myeloid malignancy is in need of better outcomes.

Although our data suggested that spliceosomal inhibitors exert therapeutic effects on *EVI1*-r AML with *SF3B1* mutations, there is debate on whether leukemia-associated mutations in RNA splicing factors drive disease development and/or maintenance owing to mis-splicing of key mRNAs and/or via impacts on cellular processes distinct from RNA splicing.[38,49] It will therefore be very exciting to use the SF3B1 mutant models here to study the impact of correcting the individual mis-splicing event in *EVI1* as well as more global alterations in RNA splicing created by mutant SF3B1 using these models.

Acknowledgments

Inv(3) mouse strain (RBRC09508, 3q21q26 mouse line B) was kindly provided by Masayuki Yamamoto (Tohoku University) and RIKEN BRC through the National BioResource Project of the MEXT/AMED, Japan.

This work was supported by American Society of Hematology (S.C.L. and D.I.), Japanese Society of Hematology (D.I.), Leukemia & Lymphoma Society (D.I. and O.A.-W.), National Institutes of Health (NIH), National Cancer Institute grants R01 CA242020 (O.A.-W.), R01 CA251138 (O.A.-W.), and R00 CA218896 (S.C.L.), National Heart, Lung, and Blood Institute grant R01HL128239 (O.A.-W.), P50 254838 (O.A.-W.), the Edward P. Evans Foundation (O.A.-W. and S.C.L.), and the Vera and Joseph Dresner Foundation (S.C.L.). D.I. is supported by The Naito Foundation, The Uehara Memorial Foundation, Senri Life Science Foundation, The Sumitomo Foundation, The Kanae Foundation for the Promotion of Medical Science, The Mitsubishi Foundation, KAKETSUKEN, Bristol Myers Squibb Foundation, JSPS KAKENHI (JP20H00537 and JP20H03717) and AMED (21ck0106697h0001). A.T. is supported by JSPS KAKENHI (JP21J15620, 16H06279 (PAGS)).

Authorship

Contribution: A.T., D.I., and O.A.-W. designed the study; H. Kawamoto supervised retroviral experiments; J.P.B. and T.A.N. provided clinical data; D.I., W.Z., A.T., M.N., R.M.-L., A.P., and R.D. performed computational analyses of mutational/RNA-seq data; M.N., S.H., and A.P. performed computational analyses of RNA-seq data; A.Y. and M.H. performed ChIP-seq; D.I., W.Z., A.K., T.I., and M.N. performed computational analyses of ChIP-seq data; H. Kunimoto and H.N. provided YCU-AML1 cells; A.T. and B.L. performed minigene splicing assay; T.K. performed protein structural analysis; A.T., H.Y., S.H., M.K., Y.H., H.C., S.C.L., M.X., Y.K., Y.Z., W.Z., M.F., Y.A., H.H., S.C.L., and D.I. performed animal experiments; A.T., D.I., M.N., A.P., and O.A.-W. wrote the manuscript with approval from all coauthors.

Conflict-of-interest disclosure: O.A.-W. has served as a consultant for H3B Biomedicine, Foundation Medicine Inc, Merck, Janssen, and Loxo Oncology/Lilly, is on the Scientific Advisory Board of Envisagenics Inc and Harmonic Discovery Inc, and has received prior research funding from H3B Biomedicine, Loxo Oncology/Lilly, and Nurix Therapeutics unrelated to the current manuscript. D.I. has received prior research funding from Abbvie and Sumitomo Dainippon Pharma unrelated to the current manuscript. The remaining authors declare no competing financial interests.

ORCID profiles: A.T., 0000-0002-9449-4894; R.M.-L., 0000-0003-0298-7948; A.P., 0000-0003-2429-2370; A.Y., 0000-0002-5639-8068; T.K., 0000-0002-4412-2849; T.I., 0000-0002-3455-6010; D.I., 0000-0002-7947-6540.

Correspondence: Omar Abdel-Wahab, Human Oncology and Pathogenesis Program, Memorial Sloan Kettering Cancer Center, New York, NY 10045; e-mail: abdelwao@mskcc.org; Daichi Inoue, Department of Hematology-Oncology, Institute of Biomedical Research and Innovation, Foundation for Biomedical Research and Innovation at Kobe, Kobe, Japan 6500047; e-mail: d-inoue@fbri.org.

Footnotes

Submitted 28 December 2021; accepted 6 June 2022; prepublished online on *Blood* First Edition 16 June 2022. DOI 10.1182/blood.2021015325.

*O.A.-W. and D.I. contributed equally to this study.

The data reported in this article have been deposited in the Gene Expression Omnibus database (accession number GSE49642; mouse model: accession GSE190655, human cell line: GSE190653, mouse colony with retroviral EVI1 expression: GSE202208).

RNA-seq reads for the human samples reported in Leucegene were downloaded from the Gene Expression Omnibus (accession number GSE49642). RNA-seq data generated by the Beat AML data (dbGaP accession phs001657.v1.p1) were downloaded from the National Cancer Institute Genomic Data Commons. RNA-seq data generated in this study have been deposited in the Gene Expression Omnibus (mouse model: accession GSE190655, human cell line: GSE190653, mouse colony with retroviral EVI1 expression: GSE202208), and the human ChIP-seq data are deposited in GSE190652, GSE202207, and available from the investigators upon request.

The online version of this article contains a data supplement.

There is a *Blood* Commentary on this article in this issue.

The publication costs of this article were defrayed in part by page charge payment. Therefore, and solely to indicate this fact, this article is hereby marked "advertisement" in accordance with 18 USC section 1734.

REFERENCES

1. Sun J, Konoplev SN, Wang X, et al. De novo acute myeloid leukemia with inv(3)(q21q26.2) or t(3;3)(q21;q26.2): a clinicopathologic and cytogenetic study of an entity recently added to the WHO classification. *Mod Pathol.* 2011;24(3):384-389.

2. Lugthart S, Gröschel S, Beverloo HB, et al. Clinical, molecular, and prognostic significance of WHO type inv(3)(q21q26.2)/t(3;3)(q21;q26.2) and various other 3q abnormalities in acute myeloid leukemia. *J Clin Oncol.* 2010;28(24):3890-3898.

3. Cui W, Sun J, Cotta CV, Medeiros LJ, Lin P. Myelodysplastic syndrome with inv(3)(q21q26.2) or t(3;3)(q21;q26.2) has a high risk for progression to acute myeloid leukemia. *Am J Clin Pathol.* 2011;136(2):282-288.

4. Rogers HJ, Vardiman JW, Anastasi J, et al. Complex or monosomal karyotype and not blast percentage is associated with poor survival in acute myeloid leukemia and myelodysplastic syndrome patients with inv(3)(q21q26.2)/t(3;3)(q21;q26.2): a Bone Marrow Pathology Group study. *Haematologica.* 2014;99(5):821-829.

5. Gröschel S, Lugthart S, Schlenk RF, et al. High EVI1 expression predicts outcome in younger adult patients with acute myeloid leukemia and is associated with distinct cytogenetic abnormalities. *J Clin Oncol.* 2010;28(12):2101-2107.

6. Summerer I, Haferlach C, Meggendorfer M, Kern W, Haferlach T, Stengel A. Prognosis of *MECOM* (*EVI1*)-rearranged MDS and AML patients rather depends on accompanying molecular mutations than on blast count. *Leuk Lymphoma.* 2020;61(7):1756-1759.

7. Yamazaki H, Suzuki M, Otsuki A, et al. A remote GATA2 hematopoietic enhancer drives leukemogenesis in inv(3)(q21;q26) by activating EVI1 expression. *Cancer Cell.* 2014;25(4):415-427.

8. Gröschel S, Sanders MA, Hoogenboezem R, et al. A single oncogenic enhancer rearrangement causes concomitant EVI1 and GATA2 deregulation in leukemia. *Cell.* 2014;157(2):369-381.

9. Haferlach C, Bacher U, Haferlach T, et al. The inv(3)(q21q26)/t(3;3)(q21;q26) is frequently accompanied by alterations of the RUNX1, KRAS and NRAS and NF1 genes and mediates adverse prognosis both in MDS and in AML: a study in 39 cases of MDS or AML. *Leukemia.* 2011;25(5):874-877.

10. Lavallée VP, Gendron P, Lemieux S, D'Angelo G, Hébert J, Sauvageau G. EVI1-rearranged acute myeloid leukemias are characterized by distinct molecular alterations. *Blood.* 2015;125(1):140-143.

11. Gröschel S, Sanders MA, Hoogenboezem R, et al. Mutational spectrum of myeloid malignancies with inv(3)/t(3;3) reveals a predominant involvement of RAS/RTK signaling pathways. *Blood.* 2015;125(1):133-139.

12. Cheng DT, Mitchell TN, Zehir A, et al. Memorial Sloan Kettering-integrated mutation profiling of actionable cancer targets (MSK-IMPACT): a hybridization capture-based next-generation sequencing clinical assay for solid tumor molecular oncology. *J Mol Diagn.* 2015;17(3):251-264.

13. Zehir A, Benayed R, Shah RH, et al. Mutational landscape of metastatic cancer revealed from prospective clinical sequencing of 10,000 patients [published correction appears in *Nat Med.* 2017;23(8):1004]. *Nat Med.* 2017;23(6):703-713.

14. Obeng EA, Chappell RJ, Seiler M, et al. Physiologic expression of Sf3b1(K700E) causes impaired erythropoiesis, aberrant splicing, and sensitivity to therapeutic spliceosome modulation. *Cancer Cell.* 2016;30(3):404-417.

15. Tyner JW, Tognon CE, Bottomly D, et al. Functional genomic landscape of acute myeloid leukaemia. *Nature.* 2018;562(7728):526-531.

16. Inoue D, Bradley RK, Abdel-Wahab O. Spliceosomal gene mutations in myelodysplasia: molecular links to clonal abnormalities of hematopoiesis. *Genes Dev.* 2016;30(9):989-1001.

17. Yoshida K, Sanada M, Shiraishi Y, et al. Frequent pathway mutations of splicing machinery in myelodysplasia. *Nature.* 2011;478(7367):64-69.

18. Ley TJ, Miller C, Ding L, et al; Cancer Genome Atlas Research Network. Genomic and epigenomic landscapes of adult de novo acute myeloid leukemia. *N Engl J Med.* 2013;368(22):2059-2074.

19. Papaemmanuil E, Cazzola M, Boultwood J, et al; Chronic Myeloid Disorders Working Group of the International Cancer Genome Consortium. Somatic SF3B1 mutation in myelodysplasia with ring sideroblasts. *N Engl J Med.* 2011;365(15):1384-1395.

20. Malcovati L, Karimi M, Papaemmanuil E, et al. SF3B1 mutation identifies a distinct subset of myelodysplastic syndrome with ring sideroblasts. *Blood.* 2015;126(2):233-241.

21. Malcovati L, Stevenson K, Papaemmanuil E, et al. SF3B1-mutant MDS as a distinct disease subtype: a proposal from the International Working Group for the Prognosis of MDS [published correction appears in *Blood.* 2021;137(21):3003]. *Blood.* 2020;136(2):157-170.

22. Papaemmanuil E, Gerstung M, Bullinger L, et al. Genomic classification and prognosis in acute myeloid leukemia. *N Engl J Med.* 2016;374(23):2209-2221.

23. Ochi Y, Kon A, Sakata T, et al. Combined cohesin-RUNX1 deficiency synergistically perturbs chromatin looping and causes myelodysplastic syndromes. *Cancer Discov.* 2020;10(6):836-853.

24. Mupo A, Seiler M, Sathiaseelan V, et al. Hemopoietic-specific Sf3b1-K700E knock-in mice display the splicing defect seen in human MDS but develop anemia without ring sideroblasts. *Leukemia.* 2017;31(3):720-727.

25. Darman RB, Seiler M, Agrawal AA, et al. Cancer-associated SF3B1 hotspot mutations induce cryptic 3′ splice site selection through use of a different branch point. *Cell Rep.* 2015;13(5):1033-1045.

26. Shiozawa Y, Malcovati L, Gallì A, et al. Aberrant splicing and defective mRNA production induced by somatic spliceosome mutations in myelodysplasia. *Nat Commun.* 2018;9(1):3649.

27. Obeng EA, Stewart C, Abdel-Wahab O. Altered RNA processing in cancer pathogenesis and therapy. *Cancer Discov*. 2019;9(11):1493-1510.

28. Inoue D, Abdel-Wahab O. Modeling SF3B1 mutations in cancer: advances, challenges, and opportunities. *Cancer Cell*. 2016;30(3): 371-373.

29. Birdwell C, Fiskus W, Kadia TM, DiNardo CD, Mill CP, Bhalla KN. EVI1 dysregulation: impact on biology and therapy of myeloid malignancies. *Blood Cancer J*. 2021; 11(3):64.

30. Kunimoto H, Fukuchi Y, Murakami K, et al. Establishment of a high-risk MDS/AML cell line YCU-AML1 and its xenograft model harboring t(3;3) and monosomy 7. *HemaSphere*. 2020;4(5):e469.

31. Hamaguchi H, Suzukawa K, Nagata K, Yamamoto K, Yagasaki F, Morishita K. Establishment of a novel human myeloid leukaemia cell line (HNT-34) with t(3;3)(q21;q26), t(9;22)(q34;q11) and the expression of EVI1 gene, P210 and P190 BCR/ABL chimaeric transcripts from a patient with AML after MDS with 3q21q26 syndrome. *Br J Haematol*. 1997;98(2): 399-407.

32. Jumper J, Evans R, Pritzel A, et al. Highly accurate protein structure prediction with AlphaFold. *Nature*. 2021;596(7873):583-589.

33. Kataoka K, Sato T, Yoshimi A, et al. Evi1 is essential for hematopoietic stem cell self-renewal, and its expression marks hemato-poietic cells with long-term multilineage repopulating activity. *J Exp Med*. 2011; 208(12):2403-2416.

34. Uehara T, Minoshima Y, Sagane K, et al. Selective degradation of splicing factor CAPERα by anticancer sulfonamides. *Nat Chem Biol*. 2017;13(6):675-680.

35. Ottema S, Mulet-Lazaro R, Erpelinck-Verschueren C, et al. The leukemic oncogene EVI1 hijacks a MYC super-enhancer by CTCF-facilitated loops. *Nat Commun*. 2021;12(1):5679.

36. Argiropoulos B, Yung E, Humphries RK. Unraveling the crucial roles of Meis1 in leukemogenesis and normal hematopoiesis. *Genes Dev*. 2007;21(22):2845-2849.

37. Inoue D, Chew GL, Liu B, et al. Spliceosomal disruption of the non-canonical BAF complex in cancer. *Nature*. 2019;574(7778): 432-436.

38. Inoue D, Polaski JT, Taylor J, et al. Minor intron retention drives clonal hematopoietic disorders and diverse cancer predisposition. *Nat Genet*. 2021;53(5):707-718.

39. Dolatshad H, Pellagatti A, Fernandez-Mercado M, et al. Disruption of SF3B1 results in deregulated expression and splicing of key genes and pathways in myelodysplastic syndrome hematopoietic stem and progenitor cells. *Leukemia*. 2015; 29(5):1092-1103.

40. Jin S, Su H, Tran NT, et al. Splicing factor SF3B1K700E mutant dysregulates erythroid differentiation via aberrant alternative splicing of transcription factor TAL1. *PLoS One*. 2017;12(5):e0175523.

41. Furney SJ, Pedersen M, Gentien D, et al. SF3B1 mutations are associated with alternative splicing in uveal melanoma. *Cancer Discov*. 2013;3(10):1122-1129.

42. Alsafadi S, Houy A, Battistella A, et al. Cancer-associated SF3B1 mutations affect alternative splicing by promoting alternative branchpoint usage. *Nat Commun*. 2016;7(1): 10615.

43. Wang L, Brooks AN, Fan J, et al. Transcriptomic characterization of SF3B1 mutation reveals its pleiotropic effects in chronic lymphocytic leukemia. *Cancer Cell*. 2016;30(5):750-763.

44. Tang AD, Soulette CM, van Baren MJ, et al. Full-length transcript characterization of SF3B1 mutation in chronic lymphocytic leukemia reveals downregulation of retained introns. *Nat Commun*. 2020;11(1):1438.

45. Gupta I, Collier PG, Haase B, et al. Single-cell isoform RNA sequencing characterizes isoforms in thousands of cerebellar cells. *Nat Biotechnol*. 2018;36(12):1197-1202.

46. Steensma DP, Bejar R, Jaiswal S, et al. Clonal hematopoiesis of indeterminate potential and its distinction from myelodysplastic syndromes. *Blood*. 2015; 126(1):9-16.

47. McKerrell T, Park N, Moreno T, et al; Understanding Society Scientific Group. Leukemia-associated somatic mutations drive distinct patterns of age-related clonal hemopoiesis. *Cell Rep*. 2015;10(8): 1239-1245.

48. Germeshausen M, Ancliff P, Estrada J, et al. MECOM-associated syndrome: a heterogeneous inherited bone marrow failure syndrome with amegakaryocytic thrombocytopenia. *Blood Adv*. 2018;2(6): 586-596.

49. Chen L, Chen JY, Huang YJ, et al. The augmented R-loop is a unifying mechanism for myelodysplastic syndromes induced by high-risk splicing factor mutations. *Mol Cell*. 2018;69(3):412-425.e6.